ISSN 1028-334X, Doklady Earth Sciences, 2006, Vol. 408, No. 4, pp. 538–541. © Pleiades Publishing, Inc., 2006.
Original Russian Text © E.B. Sal'nikova, A.B. Kotov, V.I. Kazansky, V.A. Glebovitsky, N.N. Pertsev, S.Z. Yakovleva, A.M. Fedoseenko, Yu.V. Plotkina, 2006, published in Doklady Akademii Nauk, 2006, Vol. 408, No. 4, pp. 503–507.

GEOLOGY

Early Proterozoic Age of the Tyrkandin Fault Zone, the Aldan Shield: U–Pb Dating of Fragments of Single Zircon Grains

E. B. Sal'nikova[a], A. B. Kotov[a], V. I. Kazansky[b], Corresponding Member of the RAS V. A. Glebovitsky[b], N. N. Pertsev[a], S. Z. Yakovleva[a], A. M. Fedoseenko[a], and Yu. V. Plotkina[b]

Received February 7, 2006

DOI: 10.1134/S1028334X06040076

In recent years, we have obtained numerous geochronological data that make it possible to constrain the timing of major mapable structures in the central Aldan Shield [1, 2]. Unfortunately, such data are still absent for the eastern part of this region. Therefore, it is difficult to elaborate integrated geodynamic models of the evolution of Precambrian complexes of the Siberian Craton basement.

This paper is devoted to geochronological study of the Tyrkandin fault zone, which is one of the largest sutures in the eastern Aldan Shield (Fig. 1). This 20-km-wide zone extends more than 500 km. It is characterized by positive magnetic linear anomalies. In addition, the zone coincides with a large gravity step, which separates blocks with different structures of the earth's crust. It should also be noted that the Tyrkandin fault zone hosts numerous mafic and ultramafic bodies. In addition, unlike surrounding granulites, K- and K–Na-granitoids, which are widespread in this zone, form migmatite leucosome, pegmatoid granite veins, and concordant granite gneiss and gneissic granite bodies.

Maksimov et al. [3] distinguished at least four stages in the geological evolution of the Tyrkandin fault zone. The first stage was responsible for the formation of granulite-facies blastocataclasites and blastomylonites. The second and third stages produced amphibolite-facies blastocataclasites and blastomylonites, as well as quartz–feldspar and pegmatoid feldspar metasomatites. The final stage was marked by diaphthoresis of the greenschist facies.

[a] *Institute of Precambrian Geology and Geochronology, Russian Academy of Sciences, nab. Makarova 2, St. Petersburg, 199034 Russia; e-mail: akotov@peterlink.ru*

[b] *Institute of Geology of Ore Deposits, Petrography, Mineralogy, and Geochemistry, Russian Academy of Sciences, Staromonetnyi per. 35, Moscow, 119017 Russia; e-mail: vkazansky@mtu-net.ru*

In order to determine the timing of the Tyrkandin fault zone based on the U–Pb geochronological investigation, we took quartz–feldspar and feldspar metasomatites, which, as mentioned above, formed at the late stages of its evolution. The metasomatites form various (in size and shape) bodies, which extend along the Tyrkandin zone, but they also often crosscut banding and schistosity in the blastomylonites. They are characterized by the absence of magmatic textures, as well as the irregular and vein-type distribution of constituent minerals. The metasomatites are often confined to blastocataclasite and blastomylonite zones, where small lens-like quartz and orthoclase veinlets gradually grow and replace protolith minerals.

Sample (DZh-10/8) of vaguely banded pegmatoid feldspar metasomatites (Fig. 1) was taken for geochronological investigation. The metasomatites developed after charnockites and two-pyroxene crystalline schists, which predate the Tyrkandin fault zone. They are made up of plagioclase (bytownite–andesine, 30–90%), orthoclase (10–70%), green spinel, garnet (Alm 0.61, Prp 0.31, Sps 0.03, Grs 0.05%), corundum, and bright brown Ti-biotite (TiO_2 5.5 wt %). Mafic minerals account for no more than 15%. Accessory minerals are graphite, ilmenite, and zircon.

The accessory zircons were extracted from metasomatites following the conventional technique with the use of heavy liquids. The U–Pb geochronological study was conducted with single grains using the cathodoluminescence control (CLC) method [4] and modified method of fragmentation of single zircon grains [5]. U–Pb dating was accomplished on approximately one-half of a zircon grain or its fragment, which were extracted from the sample for cathodoluminescence analysis. The zircons were preliminarily air-abraded following the Krogh technique [6].

The selected zircon or its fragment were subjected to stepwise removal of surface contamination in alcohol, acetone, and 1 M HNO_3. After each procedure, the zircon grain or its fragment was washed in analytically

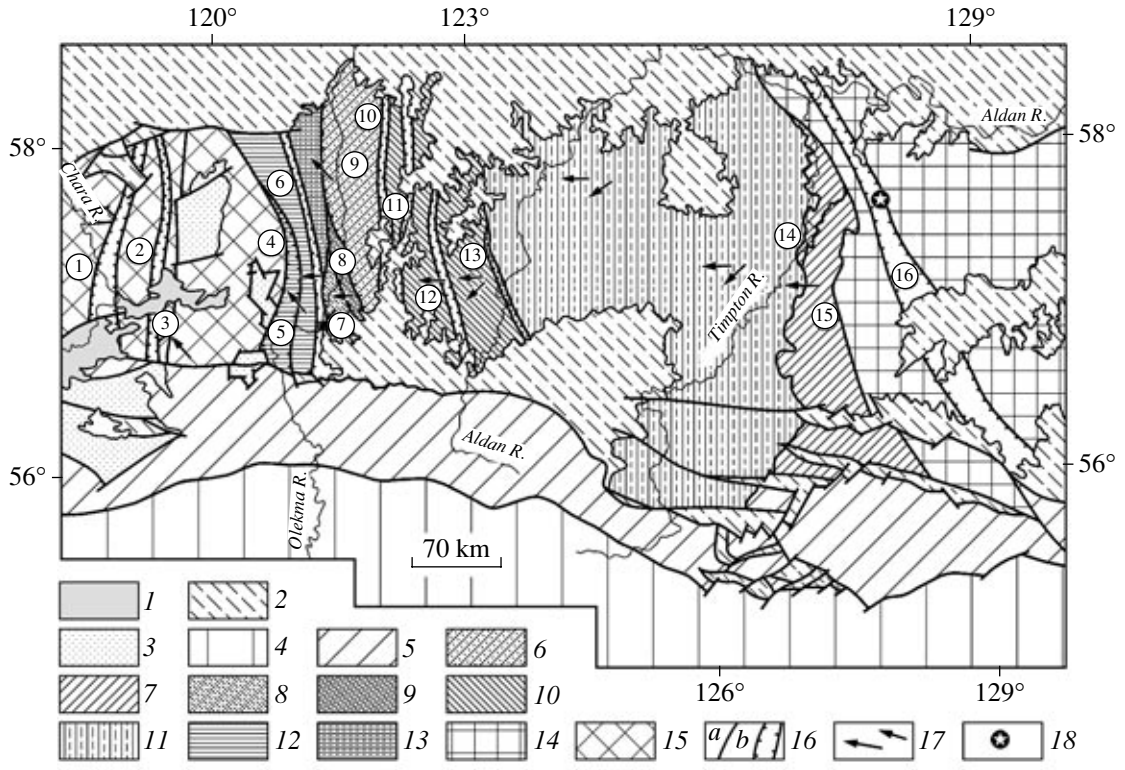

Fig. 1. Main mappable structures of the central Aldan Shield [1, 2]. (*1*) Cenozoic rocks; (*2*) Mesozoic, Paleozoic, and Upper Proterozoic platformal rocks; (*3*) Udokan Complex; (*4*) Dzhugdzhur–Stanovoi fold zone; (*5*) junction of the Aldan Shield and Dzhugdzhur–Stanovoi fold zone; (*6–13*) field of structures related to the formation of overthrust systems: (*6*) East Olekma, (*7*) Timpton, (*8*) Tungurchakan, (*9*) Chenchen, (*10*) Chugino, (*11*) Fedorov, (*12*) Temulyakit, (*13*) Tungurchin; (*14, 15*) field of (*14*) Early Proterozoic structures in the eastern Aldan geoblock and (*15*) Early Proterozoic and Late Archean structures in the eastern Chara–Olekma geoblock; (*16*) faults (*a*) and fault zones (*b*); (*17*) direction of tectonic transport during deep-seated overthrusts; (*18*) sampling site (DZh-10/8) for geochronological study. Numbers in circles denote faults and fault zones: (1) Chara–Tokko, (2) Taryn–Yuryakh, (3) East Olondo, (4) Olomokit, (5) Temulyakit, (6) Tungurchin, (7) Tungurchakan, (8) Chenchen, (9) East Olekma, (10) Borsalin–Nelyukin, (11) Amga, (12) Chugino–Amedichin, (13) Aldan–Kilier, (14) Timpton, (15) Idzhek–Sutam, (16) Tyrkandin.

pure water. The decomposition of zircon and extraction of U and Pb were conducted by the modified Krogh method [7]. The Pb blank during experiment did not exceed 20 pg. Pb and U isotopic compositions were determined on a Finnigan MAT-261 mass spectrometer in static or jumping mode with the use of an electron multiplier (the discrimination coefficient for Pb was 0.32 ± 0.11 a.m.u). The experimental data were processed with the PbDAT [8] and ISOPLOT [9] programs. Ages were calculated using the conventional decay constants [10]. Corrections for the common lead were introduced in compliance with the model values [11]. All errors are given at a 2σ level.

Accessory zircon from metasomatites can be subdivided into two morphological types. Type I (80%) includes pink subhedral transparent and translucent short-prismatic, oval, and subequant crystals (Figs. 2a, 2b). They contain small, zoned, partly fractured cores (Figs. 2e–2h). Their overgrowths (80 vol % of the grain) are characterized by low birefringence, very weak zoning, and absence of luminescence (Figs. 2e–2h).

Zircon II consists of yellowish brown subhedral transparent and translucent prismatic and oval crystals (Figs. 2c, 2d). The crystals show {100} prism and {111,101, 211}, and {112} dipyramids. Their internal structure is characterized by the presence of partially recrystallized zoned prismatic "magmatic" cores and thin pale pink overgrowths with almost no luminescence (Figs. 2i–2l). In addition, some crystals contain relicts of semimetamict irregular fractured cores. The size of zircon I varies from 5 to 200 μm (K_{el} = 1.0–2.5), while zircon II ranges from 50 to 300 μm (K_{el} = 2.5–3.5).

At the first stage, zircon II was subjected to air abrasion to gather overgrowth-free cores with distinct magmatic zoning for the isotopic analysis. The results are presented in Fig. 3. and table. One data point (no. 1) is plotted in concordia with a concordia age of 1953 ± 5 Ma (MSWD = 0.62, probability of concordance 0.43). The data points of eight grains (no. 2) are plotted near concordia (discordance 1.6%) corresponding to 1943 ± 8 Ma ($^{207}Pb/^{206}Pb$). All cores of zircon II (nos. 1–3) define a discordia with the upper intercept at 1951 ± 66 Ma and the lower intercept at 286 ± 1400 Ma (MSWD = 3.1).

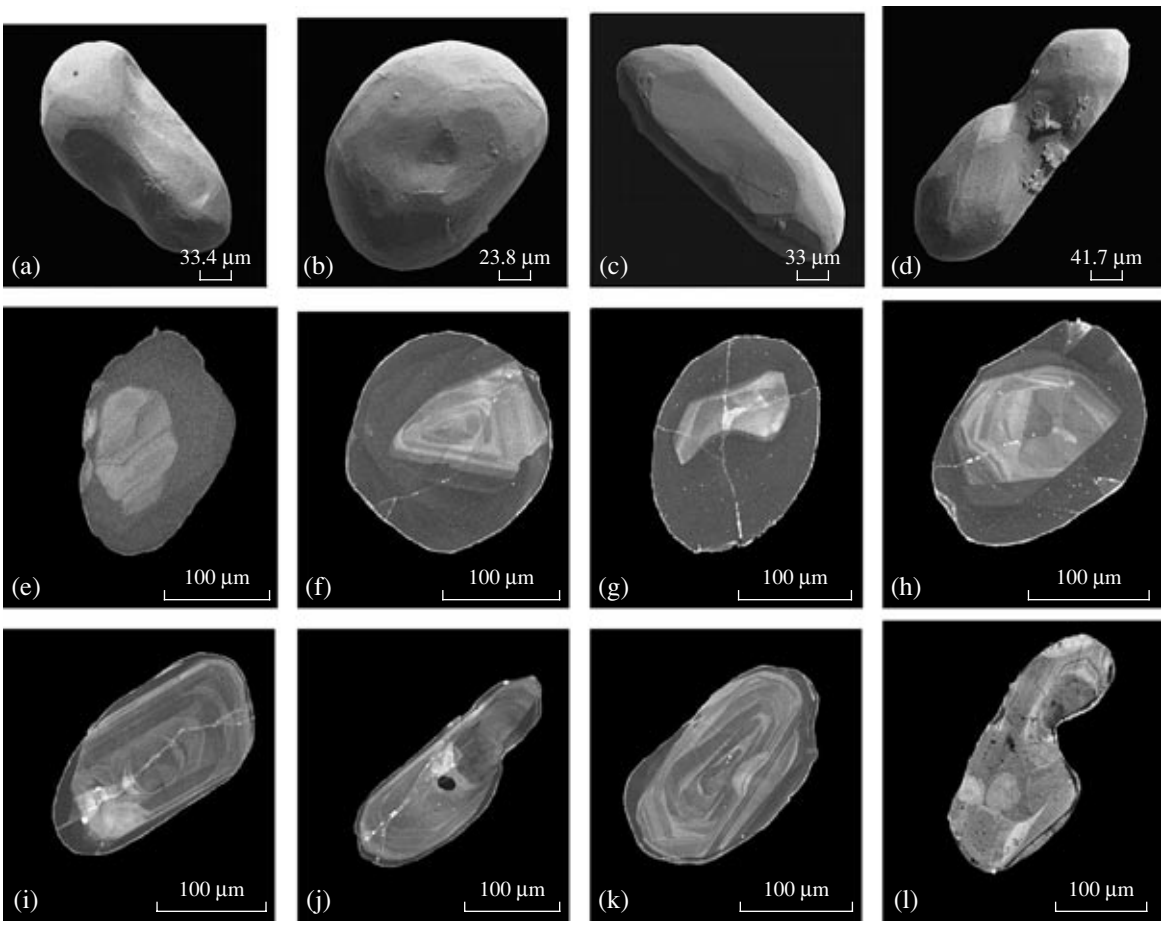

Fig. 2. Microimages of zircon crystals from sample DZh-10/8. Secondary images taken with an ABT scanning electron microscope: (a, b) zircon I, (c, d) zircon II; cathodoluminescence images taken with a Camscan scanning electron microscope: (e–h) zircon I (i–l) zircon II.

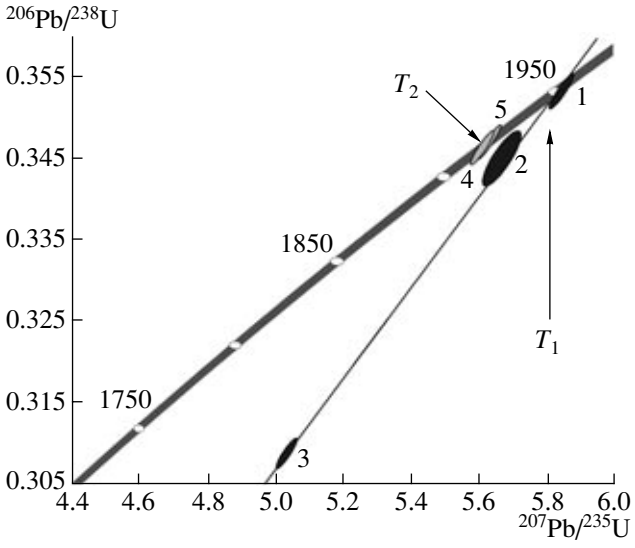

Fig. 3. Concordia diagram for zircons from feldspathic metasomatites of the Tyrkandin fault zone (sample DZh-10/8). T_1 = 1953 ± 5 Ma, T_2 = 1919 ± 4 Ma. Sample numbers correspond to the ordinal numbers in the table.

Overgrowths (nos. 4, 5) fragmented from two grains of zircon I have concordant U/Pb ratios, with a concordia age of 1919 ± 4 Ma (MSWD = 0.06, probability of concordance of 0.81).

The morphology and internal structure suggest that zircon II is a product of the partial recrystallization of magmatic zircon of charnockites and/or orthoschists during the formation of feldspar metasomatites, whereas zircon I is metasomatic phase. Hence, the concordant age of 1919 ± 4 Ma for the overgrowths of zircon I reflects the timing of the studied metasomatites and corresponds to final stages of the formation of the Tyrkandin fault zone. The concordant age of 1953 ± 5 Ma obtained for the cores of zircon II corresponds to the crystallization age of charnockites and/or orthoschists replaced by metasomatites. Therefore, the latter value corresponds to the lower age boundary of the fault zone.

Obtained data indicate that the Tyrkandin fault zone is coeval to the Timpton thrust (1925 ± 5 to 1950 ± 2 Ma) and the Amga fault zone (1925 ± 5 to 1966 ± 4 Ma) (Fig. 1) [1, 2]. Therefore, we can conclude that, like the

Results of U–Pb isotopic study of single zircon grains and their fragments from feldspathic metasomatite of the Tyrkandin fault zone (sample DZh-10/8)

Ord. no.	Grain size (μm) and its characteristics	U/Pb(a)	Isotopic ratios			
			Th/U(b)	$^{206}Pb/^{204}Pb$	$^{207}Pb/^{206}Pb$(c)	$^{208}Pb/^{206}Pb$(c)
1	<200, II, 1g, A50%, Fig. 2i	2.72	0.30	3063	0.1199 ± 2	0.0852 ± 1
2	<200, II, 8g, A30%	2.66	0.36	554	0.1189 ± 5	0.1038 ± 1
3	>100, II, 3g, A60%	3.08	0.34	1909	0.1183 ± 2	0.0961 ± 1
4	<200, I, overgrowth, 1g, Fig. 2d	2.81	0.26	5481	0.1175 ± 1	0.0745 ± 1
5	<200, I, overgrowth, 1g, Fig. 2g	2.76	0.27	1678	0.1177 ± 2	0.0774 ± 1

Ord. no.	Grain size (μm) and its characteristics	Isotopic ratios		*Rho*	Age, Ma		
		$^{207}Pb/^{235}U$	$^{206}Pb/^{238}U$		$^{207}Pb/^{235}U$	$^{206}Pb/^{238}U$	$^{207}Pb/^{206}Pb$
1	<200, II, 1g, A50%, Fig. 2i	5.8418 ± 222	0.3533 ± 12	0.92	1953 ± 7	1950 ± 7	1955 ± 3
2	<200, II, 8g, A30%	5.6667 ± 448	0.3450 ± 26	0.84	1926 ± 15	1911 ± 15	1943 ± 8
3	>100, II, 3g, A60%	5.0376 ± 212	0.3088 ± 12	0.91	1826 ± 8	1735 ± 7	1931 ± 3
4	<200, I, overgrowth, 1g, Fig. 2d	5.6105 ± 186	0.3464 ± 11	0.93	1918 ± 6	1917 ± 6	1918 ± 2
5	<200, I, overgrowth, 1g, Fig. 2g	5.6299 ± 257	0.3470 ± 15	0.95	1921 ± 9	1920 ± 8	1921 ± 3

Note: (a) The weight of zircon grain was not determined, the U/Pb ratio was determined for an arbitrarily weighed sample; (b) the Th/U ratio was calculated from $^{208}Pb/^{206}Pb$ ratio with allowance for $^{207}Pb/^{206}Pb$ age; (c) isotopic ratios corrected for procedure blank and common lead. *Rho* the correlation coefficient between $^{207}Pb/^{235}Pb$ and $^{206}Pb/^{238}Pb$; (A 50%) the amount of zircon removed by air abrasion treatment [8]; (I, II) morphological types of zircons; (1g) number of analyzed grains. The values of errors (2σ) correspond to the last significant digit.

aforesaid faults, this zone is related to the collision of the Olekma–Aldan continental microplate and passive margin of the Uchur continental microplate at the final stage of the Early Precambrian geological evolution of the Aldan Shield [1].

ACKNOWLEDGMENTS

This work was supported by the Russian Foundation for Basic Research (project nos. 04-05-64810, 05-05-65081, and 05-05-65128), the Federal Program for the Support of the Leading Scientific Schools (project no. NSh-615.2003.05), the Division of Earth Sciences of the Russian Academy of Sciences (program "Isotope Geology: Geochronology and Sources of Matter"), and the Russian Science Support Foundation.

REFERENCES

1. A. B. Kotov, Doctoral Dissertation in Geology and Mineralogy (St. Petersburg, 2003).
2. A. B. Kotov, V. A. Glebovitsky, V. I. Kazansky et al., Dokl. Akad. Nauk **404**, 799 (2005) [Dokl. Earth Sci. **405**, 1155 (2005)].
3. E. P. Maksimov, V. A. Boronikhin, L. P. Gordienko et al., in *Internal Structure of Precambrian Ore-Bearing Faults* (Nauka, Moscow, 1985), pp. 137–165 [in Russian].
4. U. Poller, V. Liebetau, and W. Todt, Chem. Geol. **139**, 287 (1997).
5. R. H. Steiger, R. A. Bickel, and V. Meier, Earth Planet. Sci. Lett. **15**, 197 (1993).
6. T. E. Krogh, Geochim. Cosmochim. Acta **46**, 637 (1982).
7. T. E. Krogh, Geochim. Cosmochim. Acta **37**, 485 (1973).
8. K. R. Ludwig, U.S. Geol. Surv. Open-File Rept. **88-542** (1999).
9. K. R. Ludwig, Berkley Geochronol. Center Spec. Publ., No. 1a (1999).
10. R. H. Steiger and E. Jager, Earth Planet. Sci. Lett. **36**, 359 (1976).
11. J. S. Stacey and I. D. Kramers, Earth Planet. Sci. Lett. **26**, 207 (1975).